Geosci. Model Dev. Discuss., https://doi.org/10.5194/gmd-2018-260
Manuscript under review for journal Geosci. Model Dev.
Discussion started: 5 November 2018

Geoscientific Model Development Discussions

The Matsuno baroclinic wave test case

Ofer Shamir[1], Itamar Yacoby[1], and Nathan Paldor[1]

[1]Fredy and Nadine Herrmann Institute of Earth Sciences, Edmond J. Safra Campus, Givat Ram, The Hebrew University of Jerusalem, Jerusalem, Israel

Correspondence: Nathan Paldor (nathan.paldor@huji.ac.il)

Abstract. The analytic wave-solutions obtained by Matsuno (1966) in his seminal work on equatorial waves provide a simple and informative way of assessing atmospheric and oceanic models by measuring the accuracy with which they simulate these waves. These solutions approximate the solutions of the shallow water equations on the sphere for small speeds of gravity waves such as those of the baroclinic modes in the atmosphere and ocean. This is in contrast to the solutions of the non-divergent barotropic vorticity equation, used in the Rossby-Haurwitz test case, which are only accurate for large speeds of gravity waves such as those of the barotropic mode. The proposed test case assigns specific values to the wave-parameters (gravity wave speed, zonal wave-number, meridional wave-mode and amplitude) for both planetary and inertia gravity waves, and confirms the accuracy of the simulation by employing Hovmöller diagrams and temporal and spatial spectra. The proposed test case is successfully applied to a standard finite-difference, equatorial, non-linear, shallow water model in spherical coordinates, which demonstrates that Matsuno's wave-solutions can be accurately simulated for at least 10 wave-periods, which for oceanic planetary waves is nearly 1300 days. In order to facilitate the use of the proposed test case, we provide Matlab, Python and Fortran codes for computing the analytic solutions at any time on arbitrary latitude-longitude grids.

1 Introduction

A cornerstone of global-scale model assessment is the Rossby-Haurwitz test case, originally used by Phillips (1959) as a qualitative way of assessing his shallow water model. Phillips initialized his model with an analytic wave-solution of the non-divergent barotropic vorticity equation obtained by Haurwitz (1940), and examined the spatio-temporal smoothness of the simulated fields at later times. Using this procedure he concluded that the emergent noise in his model was due to a small but significant divergence field missing from the initial fields. Even though the solutions of the non-divergent barotropic vorticity equation are not solution of the Shallow Water Equations (SWEs), Phillips' procedure was adopted by Williamson et al. (1992) as a standard test case for shallow water models and has been extensively used ever since (Jablonowski et al., 2009; Mohammadian and Marshall, 2010; Bosler et al., 2014; Ullrich, 2014; Li et al., 2015, are only five recent examples).

Recently, Shamir and Paldor (2016) proposed a similar procedure to that of Phillips (1959) where, instead of using the solutions of the non-divergent barotropic vorticity equation, the initial fields are taken from the analytic wave-solutions of the

Geosci. Model Dev. Discuss., https://doi.org/10.5194/gmd-2018-260
Manuscript under review for journal Geosci. Model Dev.
Discussion started: 5 November 2018

linearized SWEs on the sphere obtained by Paldor et al. (2013). These solutions account for the small but significant divergence field and can be evaluated on arbitrary latitude-longitude grids. In particular, they include the fast propagating Inertia Gravity (IG) waves, which are completely filtered out by the non-divergent barotropic vorticity equation. Consequently, the procedure proposed by Shamir and Paldor provides a more quantitative assessment than Phillips's original procedure, and is just as easy to implement.

Both solutions obtained by Haurwitz (1940) and Paldor et al. (2013) approximate the solutions of the SWEs in the asymptotic limit of large speed of gravity waves. For most practical purposes they are sufficiently accurate for speeds of gravity waves of about $200-300$ ms^{-1} or higher, which are typical of the barotropic mode in Earth's atmosphere and oceans. However, typical speeds of gravity waves of baroclinic modes are about $20-30$ ms^{-1} for the (tropical) atmosphere (Wheeler and Kiladis, 1999) and $2-3$ ms^{-1} for the oceans (Chelton et al., 1998). Thus, the above procedures are only relevant for assessing the accuracy with which the barotropic wave mode is resolved. In order to assess the accuracy of the baroclinic wave modes we propose, in the present work, to use the analytic wave-solutions of the linearized SWEs on the equatorial β-plane obtained by Matsuno (1966), which approximate the solutions of the SWEs on the sphere in the asymptotic limit of small speed of gravity waves (De-Leon and Paldor, 2011; Garfinkel et al., 2017).

In addition to being on two opposite ends of the spectrum in terms of the relevant speeds of gravity wave, the solutions obtained by Matsuno (1966) differ from those obtained by both Haurwitz (1940) and Paldor et al. (2013) in their meridional extent. The former become negligible outside a narrow equatorial band, whereas the latter two have non-negligible amplitudes in the vicinity of the poles. Thus, while the Rossby-Haurwitz test case is only relevant to global-scale models, the test case proposed in the present study is applicable to both global-scale and tropical models.

A homonymous, but unrelated, test case is the baroclinic wave test case developed in Jablonowski (2004) and Jablonowski and Williamson (2006) and independently in Polvani et al. (2004), and its variants in Lauritzen et al. (2010) and Ullrich et al. (2014). This test case is concerned with the non-linear generation of synoptic-scale eddies in multi-layer models via baroclinic instability. In contrast, the proposed test case is concerned with linear wave propagation in (non-linear) single-layer models. While the customary use of the term baroclinic is associated with density variations in the vertical direction, here the same term is used to denote thin layers of fluid of homogeneous density where the gravity waves speeds are similar to those observed in baroclinic modes in the atmosphere and oceans.

The idea of using Matsuno's solutions as a test case in a similar fashion to that of the Rossby-Haurwitz test case is most likely not original, but has never been standardized. Thus, the purpose of the present work is to standardize the Matsuno test case in the same spirit that Williamson et al. (1992) standardized the Rossby-Haurwitz one. We start with a short description of the analytic expressions derived by Matsuno (1966) in section 2. The proposed test procedure, including the choice of wave-parameters and assessment criteria, is described in Section 3. We then demonstrate the usefulness of the proposed test case in section 4, using a standard finite-difference, equatorial, (non-linear) shallow water model in spherical coordinates.

Geosci. Model Dev. Discuss., https://doi.org/10.5194/gmd-2018-260
Manuscript under review for journal Geosci. Model Dev.
Discussion started: 5 November 2018

Geoscientific Model Development Discussions
Open Access
EGU

2 The analytic solutions

The proposed test case is based on the analytic solutions of the SWEs on the equatorial β-plane obtained by Matsuno (1966). These solutions have the form of zonally propagating waves, i.e.

$$\begin{bmatrix} u(x,y,t) \\ v(x,y,t) \\ \Phi(x,y,t) \end{bmatrix} = \begin{bmatrix} \hat{u}(y) \\ \hat{v}(y) \\ \hat{\Phi}(y) \end{bmatrix} e^{i(kx-\omega t)} \tag{1}$$

where x and y are the local Cartesian coordinates in the zonal and meridional directions, respectively; t is time; u and v are the velocity components in the zonal and meridional directions, respectively; Φ is the geopotential height; k is the zonal wavenumber; ω is the wave-frequency; and $\hat{u}(y), \hat{v}(y)$ and $\hat{\Phi}(y)$ are the latitude dependent amplitudes. In accordance with the sign convention used in Matsuno we assume k is non-negative and let ω take any real value. Note, however, that the sign in front of ω in (1) is opposite to that in Matsuno's theory. The convention chosen here is more intuitive as it implies that positive values of ω correspond to waves that propagate in the positive x direction, i.e. in the eastward direction.

The unknown wave-frequencies and latitude dependent amplitudes are derived from the (well-known) energies and eigenfunctions of the (time-independent) Schödinger equation of the quantum harmonic oscillator. The resulting frequencies are given by the solutions of the following cubic equation

$$\omega_{n,k}^3 - \left[gHk^2 + \frac{2\Omega\sqrt{gH}}{a}(2n+1) \right] \omega_{n,k} - \frac{2\Omega gHk}{a} = 0, \tag{2}$$

for $n = -1, 0, 1, 2, \ldots$, where Ω and a are Earth's angular frequency and mean radius, respectively; g and H are the reduced gravity and equivalent depth.

For $n \geq 1$ Equation (2) has three distinct real roots corresponding to a slowly westward propagating Rossby wave, a fast Eastward propagating Inertia Gravity (EIG) wave, and a fast Westward propagating Inertia Gravity (WIG) wave. For $n = 0$ one of the three roots, the one corresponding to a westward propagating gravity wave with $\omega = -\sqrt{gH}k$, leads to infinite zonal wind and is thus discarded as a physically reasonable solution. The remaining two roots correspond to the lowest (i.e. $n = 0$) EIG wave and the Mixed Rossby-Gravity (MRG) wave. For $n = -1$ Equation (2) has one real root $\omega = \sqrt{gH}k$, which correspond to the equatorial Kelvin wave (see Matsuno, 1966).

Geosci. Model Dev. Discuss., https://doi.org/10.5194/gmd-2018-260
Manuscript under review for journal Geosci. Model Dev.
Discussion started: 5 November 2018

Geoscientific Model Development Discussions

Having found (one of) the wave-frequencies for a given combination of n and k, the corresponding latitude dependent amplitudes can be written as

$$\hat{v}_n = \psi_n \tag{3a}$$

$$\hat{u}_{n,k} = \frac{\sqrt{gH}\epsilon^{1/4}}{ia(\omega_{n,k}^2 - gHk^2)}\left[-\sqrt{\frac{n+1}{2}}\left(\omega_{n,k} + \sqrt{gH}k\right)\psi_{n+1} - \sqrt{\frac{n}{2}}\left(\omega_{n,k} - \sqrt{gH}k\right)\psi_{n-1}\right] \tag{3b}$$

$$\hat{\Phi}_{n,k} = \frac{gH\epsilon^{1/4}}{ia(\omega_{n,k}^2 - gHk^2)}\left[-\sqrt{\frac{n+1}{2}}\left(\omega_{n,k} + \sqrt{gH}k\right)\psi_{n+1} + \sqrt{\frac{n}{2}}\left(\omega_{n,k} - \sqrt{gH}k\right)\psi_{n-1}\right], \tag{3c}$$

for $n = 1, 2, 3, \ldots$ (the cases $n = -1, 0$ require special treatment), where

$$\psi_n = AH_n\left[\epsilon^{1/4}\left(\frac{y}{a}\right)\right]\exp\left[-\frac{1}{2}\epsilon^{1/2}\left(\frac{y}{a}\right)^2\right]. \tag{4}$$

Here $\epsilon = (2\Omega a)^2/gH$ is Lamb's parameter, A is an arbitrary amplitude, and $\hat{H}_n$ are the normalized Hermite polynomials of degree n. Note: (i) The chosen normalization for the latitude dependent amplitudes in (3) is different from the one used in Matsuno. We use the above normalization for convenience, as it relates the amplitude of $\hat{v}$ to that of ψ in a straight forward way and guarantees that it is independent of both k or ω. (ii) The use of the normalized version of the Hermite polynomials also leads to slightly different pre-factors in front of ψ_{n+1} and ψ_{n-1} compared to Matsuno. However, they are generally more stable and more convenient for the spectral analyses employed in the following sections.

While the solutions obtained by Matsuno (1966) apply for the equatorial β-plane, the proposed test case is intended for use in spherical models. As is shown in Garfinkel et al. (2017), the SWEs on the equatorial β-plane approximate the SWEs on the sphere to zero-order in powers of $1/\epsilon^{1/4}$. Thus, the solutions obtained by Matsuno are only accurate in the asymptotic limit $\epsilon \to \infty$. For the fixed values of Earth's angular frequency and mean radius, this implies that the solutions obtained by Matsuno are only accurate for sufficiently small speeds of gravity waves $\sqrt{gH}$.

In practice, to use Matsuno's solutions in spherical models, the local Cartesian coordinates x and y in the above formulae (1) and (4) have to be replaced by the longitude λ and latitude ϕ of the geographical coordinate system. Recall that the transformation between the two system is $(x, y) \to a(\cos\phi_0\lambda, \phi)$, where ϕ_0 is the central latitude to which the β-plane approximation is applied. Thus, for the equatorial β-plane where $\phi_0 = 0$, the transformation is simply $(x, y) \to a(\lambda, \phi)$. Likewise, the planar wavenumber k in all of the formulae (1)-(4) has to be replace by its spherical counterpart using the transformation $k \to k/a\cos\phi_0 = k/a$.

For the small gravity wave speeds (i.e. small values of ϵ) used in the present work, the eigenfunctions in (4) become negligible outside a narrow equatorial band (see Sections 3.1 and 4 below). Thus, the above expression can be used to test both global-scale and tropical models.

Geosci. Model Dev. Discuss., https://doi.org/10.5194/gmd-2018-260
Manuscript under review for journal Geosci. Model Dev.
Discussion started: 5 November 2018

Finally, using the above formulae to calculate the waves' frequencies and latitude dependent amplitudes requires routines for finding the roots of the cubic equation (2), and for evaluating the normalized Hermite polynomials on arbitrary latitude-longitude grids. The roots of the cubic equation can be obtained in a closed analytic form using the solutions of the general cubic equation as detailed in appendix A. The normalized Hermite polynomials, in turn, can be evaluated using their three-term recurrence relation, as in Press et al. (2007). In order to facilitate the application of the proposed test case we provide as part of the online supplementary material Matlab, Python and Fortran codes (named matsuno.m, matsuno.py and matsuno.f90, respectively) for computing the analytic fields on arbitrary latitude-longitude grids.

3 Proposed test procedure

The general procedure of the proposed test case is similar to the Rossby-Haurwitz one in that the model in question is initialized with velocity and height fields corresponding to a particular wave-solution and the time evolution of that wave is then examined. The initial wave fields in this case are taken from the analytic expressions in Section 2. The specific choice of wave-parameters and assessment criteria in the present work are discussed below, separately. As is often the case, these choices represent compromises between conflicting factors, e.g. adherence to observations vs. adherence to asymptotic validity of the analytic solutions or rigorous testing vs. simplicity. In any case, these choices may be the subject of discourse as deemed appropriate by the community.

3.1 wave-parameters

The wave-parameters consist of the speed of gravity waves $\sqrt{gH}$, the wave-number and wave-mode k and n, the wave-amplitude A, and the wave-type. Any given combination of these parameters completely specify a unique wave using the expressions in (2)-(4). We consider all other parameters, including the spatio-temporal resolution and the form of diffusion/viscosity terms, to be modeling choices left to the developers. This approach is aimed at testing the models in their modus operandi. However, as noted in Polvani et al. (2004), different choices for the form of diffusion/viscosity terms correspond to different sets of equations and may not converge to the same solutions.

We offer two different choices for $\sqrt{gH}$ inspired by the observed speeds of gravity waves of the baroclinic modes in the atmosphere and oceans. In practice we keep g fixed to Earth's gravitational acceleration, and vary the speed of gravity waves by varying H. For atmospheric models we suggest using $H = 30$ m, which is within the range of observed equivalent depths in the equatorial atmosphere (Wheeler and Kiladis, 1999). For ocean models we suggest using $H = 0.5$ m, which corresponds to the observed speed of gravity waves of the first baroclinic mode in the oceans (Chelton et al., 1998). As mentioned in section 2, the analytic solutions obtained by Matsuno for the equatorial β-plane are only accurate approximations of the SWEs on the sphere in the asymptotic limit of small speeds of gravity waves. The above values were found by trial and error to be sufficiently accurate in the sense that they yield stable integrations for at least 10 wave-periods in the simulations demonstrated in Section 4.

Geosci. Model Dev. Discuss., https://doi.org/10.5194/gmd-2018-260
Manuscript under review for journal Geosci. Model Dev.
Discussion started: 5 November 2018

Geoscientific Model Development Discussions

In addition to the speed of gravity waves, the accuracy of Matsuno's solutions depend on the wave-number and wave-mode as well. For a given value of $\sqrt{gH}$, they become asymptotically accurate in the limits $k, n \to 0$ (but $k \neq 0$) (De-Leon and Paldor, 2011). In addition, the higher the wave-number or wave-mode are, the greater the spatial variability and the required spatial resolution are. Both of these considerations suggest that reasonable choices for the wave-number and wave-mode consist of small to moderate values. The proposed wave-number and wave-mode are $k = 5$ and $n = 1$, which are within the range of dominant values observed in the equatorial atmosphere (Wheeler and Kiladis, 1999), but other choices may work just as well provided k and n are not too large.

The proposed test case is based on the solutions of the linear SWEs but is intended to be used in non-linear models. Therefore, the waves-amplitude should be sufficiently small so as to satisfy the linearization condition. The proposed amplitude of Equation (4) is $A = 10^{-8}$ m s^{-1}, chosen by trial and error so as to enable stable integrations for at least 10 wave periods in the simulations in Section 4.

In general, there are two qualitatively different wave types, the Rossby and IG wave types, that differ in the magnitude of their divergence field. In order to assess the models' performances in these two qualitatively different limits we suggest using one of each. Since Rossby waves are exclusively westward propagating, we choose the EIG wave from the two IG waves as the second one in order to eliminate potential longitudinal biases.

3.2 Assessment criteria

For sufficiently small wave-amplitudes we expect the spatio-temporal structure of the simulated solutions to be that of zonally propagating waves, i.e. $\hat{\xi}(\phi)e^{i(k\lambda-\omega t)}$ (where ξ stands for any of the dependent variables u, v or Φ), with frequency and latitude dependent amplitudes corresponding to the initial wave. In this case, it is desirable to assess the accuracy of the zonal and meridional structures of the waves independently. A fast and simple way of doing so is using Hovmöller diagrams, where the temporal change in any direction is isolated by intersecting the fields along a fixed value of the other direction. This results in the following two diagrams:

(i) A longitude-time diagram obtained by intersecting the fields at a certain latitude. The contour lines in the longitude-time plane are the set of points satisfying $k\lambda - \omega t = const$ (for some real $const$). Thus, the expected pattern for this diagram is that of straight lines whose slopes equal the wave's phase speed k/ω. In order to avoid small fluctuations in the vicinity of latitudinal zero-crossings, we recommend using latitudinal intersects at or near local extrema.

(ii) A latitude-time diagram obtained by intersecting the fields at a certain longitude. For any two wave-fronts with equal phase $k(\lambda_2 - \lambda_1) = \omega(t_2 - t_1)$. Thus, holding λ fixed while varying t from t_1 to t_2 is equivalent to holding t fixed and varying λ from λ_1 to $\lambda_2 = \lambda_1 + \omega/k(t_2 - t_1)$. The resulting pattern is similar to that of a latitude-longitude diagram, but provides a testament of the time evolution as opposed to a momentary snapshot.

For a more quantitative assessment we suggest using a combination of Fourier analyses in longitude and time and a Hermite analysis in latitude to determine the dominant wave-numbers and wave-frequencies, and the dominant wave-modes (which determine the dominant meridional structure) of the simulated solution, respectively. The amplitude of the most dominant wave-component in each case can be compared to the amplitude of the analytic solution at the corresponding intersect, and

Geosci. Model Dev. Discuss., https://doi.org/10.5194/gmd-2018-260
Manuscript under review for journal Geosci. Model Dev.
Discussion started: 5 November 2018

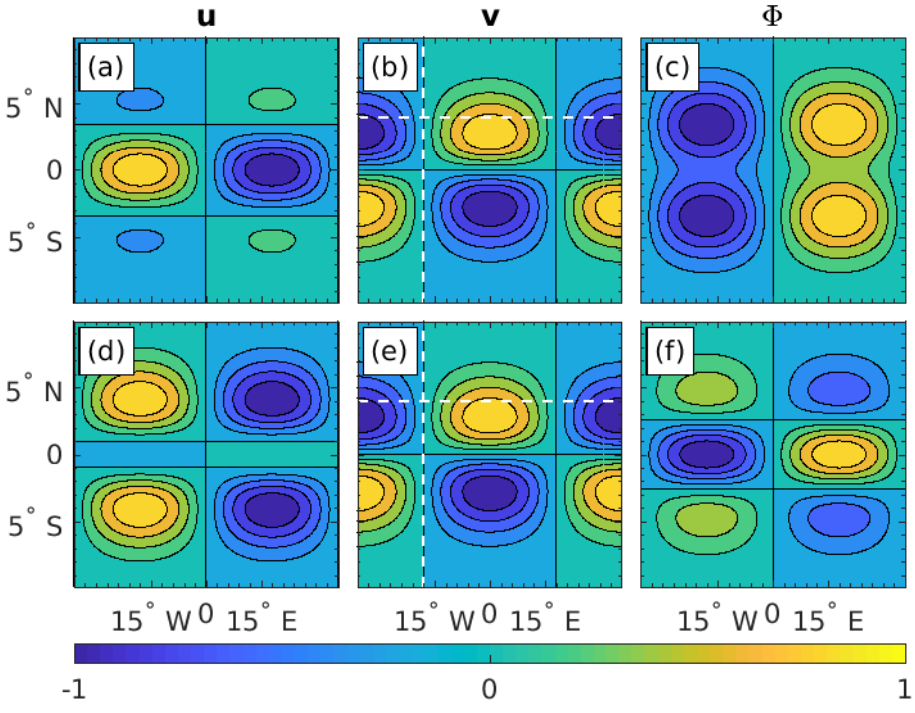

Figure 1. The initial u, v, Φ fields of the Rossby (top row) and EIG (bottom row) waves obtained using the analytic expressions of Section 2 and the parameters of Section 3.1 with $H = 0.5$ m. Each field is normalized on its own global maximum. Contour-levels range from -1.0 to $+1.0$ by 0.2. White dashed-lines (in b and e): intersects used for the Hovmöller diagrams in Figure 2.

the difference between the two provides a quantitative error-measure. The Fourier analysis can be trivially found using readily available Fast-Fourier-Transform libraries. The Hermite analysis was found in the present work using the procedure described in Appendix B.

In order to attain reasonable accuracy in terms of the spectral analysis, it is recommended to integrate the initial fields forward in time for at least 10 wave-periods, with a sampling frequency of about 10 samples per period. The proposed integration and sampling times (denoted by T_f and T_s) for each of the four simulations, along with the wave-period (denoted by T), are given in Table 1.

4 Demonstration

In order to demonstrate the usefulness of the Matsuno test case we run the proposed procedure using a simple finite-difference shallow water model. The model is a spherical version of the Cartesian model used in Gildor et al. (2016), in which the

Geosci. Model Dev. Discuss., https://doi.org/10.5194/gmd-2018-260
Manuscript under review for journal Geosci. Model Dev.
Discussion started: 5 November 2018

Geoscientific Model Development Discussions

	T (days)	T_f (days)	T_s (hours)
Rossby, $H = 30$ **m**:	18.5	200	48
EIG, $H = 30$ **m**:	1.9	20	4
Rossby, $H = 0.5$ **m**:	127.8	1300	312
EIG, $H = 0.5$ **m**:	5.7	60	12

Table 1. The wave-period T, integration time T_f, and sampling spacing T_s. Note, T is derived from the chosen test wave-parameters and is a characteristic of the waves, whereas T_f and T_s where chosen to attain reasonable accuracy in terms of the spectral analysis.

integration forward in time is carried out using the transport form of the SWEs

$$\frac{\partial U}{\partial t} + \frac{1}{a\cos\phi}\frac{\partial}{\partial\lambda}\left(\frac{U^2}{h}\right) + \frac{1}{a}\frac{\partial}{\partial\phi}\left(\frac{UV}{h}\right) - \frac{2UV\tan\phi}{ah} - 2\Omega\sin\phi V = -\frac{g}{2a\cos\phi}\frac{\partial h^2}{\partial\lambda} \tag{5a}$$

$$\frac{\partial V}{\partial t} + \frac{1}{a\cos\phi}\frac{\partial}{\partial\lambda}\left(\frac{UV}{h}\right) + \frac{1}{a}\frac{\partial}{\partial\phi}\left(\frac{V^2}{h}\right) - \frac{(U^2 - V^2)\tan\phi}{ah} + 2\Omega\sin\phi U = -\frac{g}{2a}\frac{\partial h^2}{\partial\phi} \tag{5b}$$

$$\frac{\partial h}{\partial t} + \frac{1}{a\cos\phi}\left[\frac{\partial U}{\partial\lambda} + \frac{\partial(V\cos\phi)}{\partial\phi}\right] = 0, \tag{5c}$$

where $U = hu$, $V = hv$ and h is the total layer thickness. The numerical scheme employs a standard finite difference shallow-water solver in which the time-differencing follows a leapfrog scheme (centre differencing in both time and space). The computations were done on an Arakawa C-grid. The original Matlab code used in the following simulations is available as part of the on-line supporting material.

The model's application was validated using both atmospheric and oceanic settings, i.e. using both $H = 30$ m and $H = 0.5$ m, totaling in four different initial waves (a Rossby wave and an EIG one for each value of H). The initial u, v, Φ fields of the Rossby (top row) and EIG (bottom row) waves obtained using the analytic expressions of Section 2 and the parameters of Section 3.1 are shown in Figure 1 for $H = 0.5$ m. The corresponding fields for $H = 30$ m differ only by e-folding latitude which is $11°$, instead of $4°$. Note that under the normalization of the present paper the initial v field is independent of the wave type and is therefore identical on both rows, panels (b) and (e).

In all four cases, the computational domain was $-180° \le \lambda \le 180°$ and $-30° \le \phi \le 30°$. The boundary conditions were periodicity at the zonal boundaries $\lambda = \pm 180°$ and vanishing meridional velocity at the channel's boundaries $\phi = \pm 30°$. For $H = 30$ m, the meridional velocity at $\phi = \pm 30°$ decays to $4e-03$ of its maximal value, and for $H = 0.5$ m it decays to $2e-24$ of its maximal value, so in both cases the velocity outside the computational domain can be comfortably neglected. The grid-spacing and time step were $\Delta\lambda = \Delta\phi = 0.5°$ and $\Delta t = 600$ seconds, which were found to yield stable solutions for at least 10 wave-periods.

Geosci. Model Dev. Discuss., https://doi.org/10.5194/gmd-2018-260
Manuscript under review for journal Geosci. Model Dev.
Discussion started: 5 November 2018

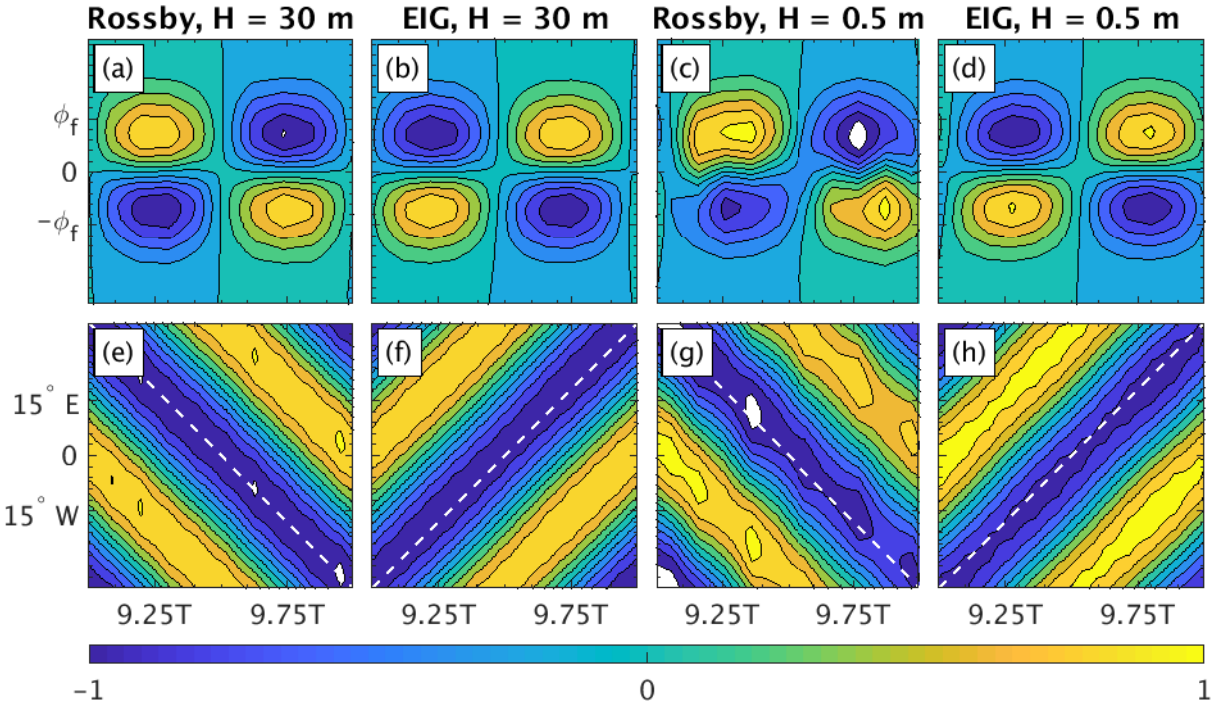

Figure 2. Hovmöller diagrams of the simulated solutions. (a)–(d) Latitude-time diagrams obtained by intersecting v at $\lambda = -18°$. (e)–(h) Longitude-time diagrams obtained by intersecting v at $\phi = 9°$ for $H = 30$ m, and $\phi = 4°$ for $H = 0.5$ m (the later case is indicated by horizontal dashed white lines in Figure 1). For the sake of legibility the shown time domain in each panel is $9T \leq t \leq 10T$, where T is the corresponding wave-period provided in Table 1. For comparison, the analytic (initial) slope in each case is indicated using dashed white line (bottom row). The amplitude in each panel is normalized on the global maximum at $t = 0$, i.e. $v/\max_{\lambda,\phi}|v(t=0)|$, which is the same in all cases. Contour-levels range from -1.0 to $+1.0$ by 0.2.

The resulting Hovmöller diagrams of the simulated solutions for each of the initial waves are shown in Figure 2. In all cases, the latitude-time diagrams were obtained by intersecting v at $\lambda = -18°$ (also indicated by vertical dashed white lines in Figure 1). The longitude-time diagrams were obtained by intersecting v at $\phi = 9°$ for $H = 30$ m, and $\phi = 4°$ for $H = 0.5$ m (the latter case is indicated by horizontal dashed white lines in Figure 1). Similar results are obtained using u or Φ, provided the meridional intersects are taken in the vicinity of their local extrema. For the sake of legibility the shown time domain in each panel is $9T \leq t \leq 10T$, where T is the corresponding wave-period provided in Table 1. Note that the latitude-time diagrams are similar to that of a latitude-longitude diagram and can, therefore, be used to compare with the initial fields. In all cases the initial wave-structure is clearly discernible after 10 wave-periods and the dominant slope corresponds to the analytic slope indicated with dashed white lines.

Geosci. Model Dev. Discuss., https://doi.org/10.5194/gmd-2018-260
Manuscript under review for journal Geosci. Model Dev.
Discussion started: 5 November 2018

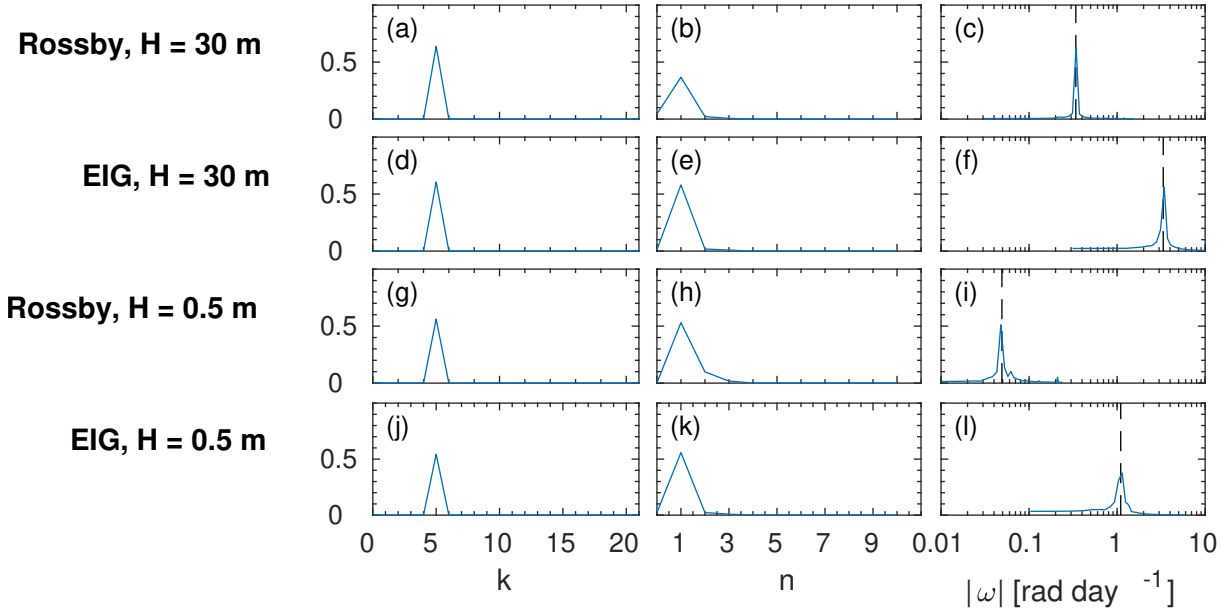

Figure 3. Power-spectra of the simulated solutions. Left column: Power-spectra in k-space obtained using Fourier analyses of longitudinal series at $(\phi,t)=(9^\circ,10T)$ and $(\phi,t)=(4^\circ,10T)$ for $H=30$ m and $H=0.5$ m, respectively, where T in each case is the corresponding wave-period provided in Table 1. Middle column: Power-spectra in n-space obtained using Hermite analyses of latitudinal series at $(\lambda,t)=(-18^\circ,10T)$. Right column: Power-spectra in ω-space obtained using Fourier analyses of time series at $(\lambda,\phi)=(-18^\circ,9^\circ)$ and $(\lambda,\phi)=(-18^\circ,4^\circ)$ for $H=30$ m and $H=0.5$ m, respectively. Since the fields are real, only a one-sided power spectrum is shown, i.e. for $|\omega|$. In order to facilitate the comparison, the initial frequencies for the chosen parameters in Section 3.1 are also indicated in the figure using black dashed lines. For the sake of presentation all power spectra are multiplied by 10^{-8}.

For a more quantitative assessment we use Fourier and Hermite analyses in order to locate the dominant wave-numbers, wave-modes, and wave-frequencies, and compare their amplitudes with the initial wave amplitudes. Figure 3 contains the resulting power-spectra of the simulated solutions obtained using the same latitudinal and longitudinal intersects used for the Hovmöller diagrams in Figure 2, and $t=10T$ as the time intersect, where T in each case is the corresponding wave-period listed in Table 1. In all cases the dominant wave-number and wave-mode clearly match the initial values $k=5$ and $n=1$. Likewise the dominant frequencies match the initial ones indicated on the figure using black dashed lines.

The first and second most dominant wave components of the simulated solutions are summarized in Table 2, compared to the wave components of the analytic (initial) solutions. The errors in the frequencies were derived from the spectral resolution, which for (about) 10 wave-periods integration is (about) 10% of the initial wave's frequency in each case. The errors in the amplitudes of the first most dominant wave components were estimated using the amplitudes of the second most dominant ones, and the errors in the amplitudes of the second most dominant wave components were estimated using the amplitudes of the third most dominant ones.

Geosci. Model Dev. Discuss., https://doi.org/10.5194/gmd-2018-260
Manuscript under review for journal Geosci. Model Dev.
Discussion started: 5 November 2018

Geoscientific Model Development Discussions

	k	$\lvert\hat{F}_k\rvert$ (m sec^{-1})	n	$\lvert\hat{F}_n\rvert$ (m sec^{-1})	$\lvert\omega\rvert$ (rad day^{-1})	$\lvert\hat{F}_\omega\rvert$ (m sec^{-1})
Rossby, $H = 30$ **m**:						
Analytic	5	6.29e-09	1	2.39e-09	3.40e-01	6.29e-09
1st most dominant	5	6.39e-09 $\pm$ 9.99e-15	1	3.68e-09 $\pm$ 4.46e-10	3.42e-01 $\pm$ 3.11e-02	6.32e-09 $\pm$ 4.90e-10
2nd most dominant	35	9.99e-15 $\pm$ 8.86e-15	0	4.46e-10 $\pm$ 2.19e-10	3.11e-01 $\pm$ 3.11e-02	4.90e-10 $\pm$ 4.44e-10
EIG, $H = 30$ **m**:						
Analytic	5	6.29e-09	1	2.83e-09	3.34e+00	6.29e-09
1st most dominant	5	6.06e-09 $\pm$ 4.53e-15	1	5.81e-09 $\pm$ 1.82e-10	3.43e+00 $\pm$ 3.12e-01	5.61e-09 $\pm$ 1.88e-09
2nd most dominant	10	4.53e-15 $\pm$ 3.95e-15	2	1.82e-10 $\pm$ 1.14e-10	3.12e+00 $\pm$ 3.12e-01	1.88e-09 $\pm$ 1.10e-09
Rossby, $H = 0.5$ **m**:						
Analytic	5	5.46e-09	1	1.17e-09	4.92e-02	5.46e-09
1st most dominant	5	5.62e-09 $\pm$ 3.27e-15	1	5.30e-09 $\pm$ 9.82e-10	4.79e-02 $\pm$ 4.79e-03	5.11e-09 $\pm$ 1.37e-09
2nd most dominant	52	3.27e-15 $\pm$ 2.87e-15	2	9.82e-10 $\pm$ 1.80e-10	5.26e-02 $\pm$ 4.79e-03	1.37e-09 $\pm$ 1.02e-09
EIG, $H = 0.5$ **m**:						
Analytic	5	5.46e-09	1	4.57e-09	1.10e+00	5.46e-09
1st most dominant	5	5.43e-09 $\pm$ 1.25e-15	1	5.58e-09 $\pm$ 2.27e-10	1.14e+00 $\pm$ 1.04e-01	3.76e-09 $\pm$ 3.11e-09
2nd most dominant	55	1.25e-15 $\pm$ 1.22e-15	2	2.27e-10 $\pm$ 2.21e-10	1.04e+00 $\pm$ 1.04e-01	3.11e-09 $\pm$ 1.16e-09

Table 2. The first and second most dominant wave components of the simulated solutions, compared to the wave components of the analytic (initial) solutions. The dominant components were obtained from the same analyses as in Figure 3, i.e. using the same series. The frequencies errors were derived from the spectral resolution, which is about 10% for the ten wave-periods integration. The errors in the amplitudes of the first most dominant wave components were estimated using the amplitudes of the second most dominant component, and the errors in the amplitudes of the second most dominant wave components were estimated using the amplitudes of the third most dominant component. $\lvert\hat{F}_k\rvert$, $\lvert\hat{F}_n\rvert$ and $\lvert\hat{F}_\omega\rvert$ denote the amplitudes of the wave component in the k, n and ω spaces, respectively.

The overall scenario that emerges from the spectral analyses is similar to that of the Hovmöller diagrams, namely that the initial waves remain dominant after 10 wave-periods. However, it provides a quantitative measure of the errors in the simulated solutions, since for an ideal model the amplitudes of the first most dominant wave components should be the same as the analytic ones. Thus, the closer the amplitudes of the first most dominant wave components to the analytic ones, and the smaller the amplitudes of the second most dominant wave components, the better.

5 Concluding remarks

As vertical resolutions in atmospheric and oceanic models increase it is essential to assess the accuracy with which they resolve baroclinic wave modes, in addition to the barotropic mode. To this end we propose to use a similar procedure to the one used in the Rossby-Haurwitz test case but replace the initial conditions. Instead of using the analytic solutions obtained by Haurwitz (1940), which are only accurate for large gravity wave speeds such as those of the barotropic mode, we propose to

Geosci. Model Dev. Discuss., https://doi.org/10.5194/gmd-2018-260
Manuscript under review for journal Geosci. Model Dev.
Discussion started: 5 November 2018

Geoscientific Model Development Discussions
Open Access
EGU

use the analytic solutions obtained by Matsuno (1966), which are accurate for smaller gravity wave speeds such as those of the baroclinic modes.

Unlike the solutions obtained by Haurwitz (1940) for the non-divergent barotropic vorticity equation, the solutions of the SWEs obtained by Matsuno (1966) fully account for the velocity divergence. As a result an initial wave can be accurately simulated for long times and the simulated solution can be compared to the analytic solution to obtain a quantitative assessment. While Matsuno's solutions apply for the equatorial β-plane, they approximate the solutions of the SWEs on the sphere for the speeds of gravity waves found in the baroclinic modes in the atmosphere and oceans, and as demonstrated in the present work can be accurately simulated in spherical coordinate models. Finally, in contrast to the barotropic mode, the baroclinic modes are confined to narrow equatorial band. Therefore, the proposed test can also be used to test tropical models.

Ideally, we expect the proposed test case to stand on an equal footing alongside the Rossby-Haurwitz one, but in the words of Williamson et al. (1992): "The test will only become standard to the extent that the community finds it useful".

Code availability. The following files are available online as part of the supplementary material of this work:

matsuno.m, matsuno.py, and matsuno.f90: In order to facilitate the application of the proposed test case we provide Matlab, Python, and Fortran codes for computing the analytic solutions obtained by Matsuno as described in section 2. The code can be used to evaluate the horizontal velocity fields u and v, in m s^{-1}, and the geopotential field Φ, in m^2 s^{-2} (or h in m), on arbitrary latitude-longitude grids for all $t \geq 0$.

shallow_water_model.m: A Matalb code containing the shallow water model used in section 4.

Appendix A: The roots of the cubic equation

For any combination of wave-number and wave-mode, k and n, the wave-frequencies are given by the three roots of the cubic equation in (2). These roots can be written in a closed analytic form using the general solution of the cubic equation (e.g. Abramowitz and Stegun, 1964):

$$\omega_{n,k,j} = -\frac{1}{3}\left(\Delta_j + \frac{\Delta_0}{\Delta_j}\right), \quad \text{for} \quad j = 1,2,3 \tag{A1}$$

where j stands for the three roots, and where

$$\Delta_0 = 3\left[gHk^2 + \frac{2\Omega\sqrt{gH}}{a}(2n+1)\right], \tag{A2a}$$

$$\Delta_j = \left[\frac{\Delta_4 + \sqrt{\Delta_4^2 - 4\Delta_0^3}}{2}\right]^{1/3} \times \exp\left(\frac{2\pi j}{3}i\right), \tag{A2b}$$

$$\Delta_4 = -\frac{54\Omega gHk}{a}. \tag{A2c}$$

Geosci. Model Dev. Discuss., https://doi.org/10.5194/gmd-2018-260
Manuscript under review for journal Geosci. Model Dev.
Discussion started: 5 November 2018

Geoscientific Model Development Discussions
Open Access
EGU

Given the definitions in (A2), the explicit expressions for the frequencies of the Rossby, WIG and EIG waves are obtained by sorting the values in (A1) as follows:

$$\text{Rossby :} \qquad \omega_{n,k,\mathrm{R}} = -\min_{j=1,2,3} |\omega_{n,k,j}|, \tag{A3a}$$

$$\text{Westward Inertia-Gravity :} \qquad \omega_{n,k,\mathrm{WIG}} = \min_{j=1,2,3} \omega_{n,k,j}, \tag{A3b}$$

$$\text{Eastward Inertia-Gravity :} \qquad \omega_{n,k,\mathrm{EIG}} = \max_{j=1,2,3} \omega_{n,k,j}. \tag{A3c}$$

Appendix B: The Hermite transform

Let $\xi(\phi)$ denote a latitudinal series (i.e. an intersect along specific longitude and time) of any one of the dependent variables. We seek approximate series expansion of the form

$$\xi(\phi) = \sum_{n=0}^{N} \hat{\xi}_n \hat{H}_n \left[\epsilon^{1/4}\phi\right] \exp\left[-\frac{1}{2}\epsilon^{1/2}\phi^2\right], \tag{B1}$$

where $\hat{\xi}_n$ are spectral coefficients, ϵ is Lamb's parameter defined in the text, and $\hat{H}_n$ are the normalized Hermite polynomials of degree n. The normalization of the Hermite polynomials implies that they are orthonormal on $[-\infty, \infty]$ with respect to the weight function $\exp(-x^2)$, i.e.

$$\int_{-\infty}^{\infty} \hat{H}_n(x)\hat{H}_m(x)e^{-x^2}\,dx = \begin{cases} 1 & \text{for } n = m \\ 0 & \text{for } n \neq m. \end{cases}$$

It follows that the spectral coefficients are given by

$$\hat{\xi}_n = \int_{-\infty}^{\infty} \xi(\phi)\hat{H}_n \left[\epsilon^{1/4}\phi\right] \exp\left[-\frac{1}{2}\epsilon^{1/2}\phi^2\right] d(\epsilon^{1/4}\phi). \tag{B2}$$

In order to apply the Hermite analysis on the finite meridional domain we assume that $\xi(\phi)$ decays sufficiently fast so that it can be approximated by zero outside the computational domain, $[-\pi/6, \pi/6]$ in the present work (or $[-\pi/2, \pi/2]$ for global-scale models). In particular, in the present work we assume that the following approximation holds

$$\int_{-\pi/6}^{\pi/6} \xi(\phi)\hat{H}_n \left[\epsilon^{1/4}\phi\right] \exp\left[-\frac{1}{2}\epsilon^{1/2}\phi^2\right] d(\epsilon^{1/4}\phi) \approx$$

$$\int_{-\infty}^{\infty} \xi(\phi)\hat{H}_n \left[\epsilon^{1/4}\phi\right] \exp\left[-\frac{1}{2}\epsilon^{1/2}\phi^2\right] d(\epsilon^{1/4}\phi).$$

Finally, the integral in (B2) was evaluated using the trapezoidal rule.

Geosci. Model Dev. Discuss., https://doi.org/10.5194/gmd-2018-260
Manuscript under review for journal Geosci. Model Dev.
Discussion started: 5 November 2018

Geoscientific Model Development Discussions
Open Access
EGU

Author contributions. NP conceived the idea of standardizing the Matsuno test case for General Circulation Models in spherical coordinates. IY adopted the Cartesian shallow water model used in Gildor et al. (2016) to spherical coordinates and was responsible for the numerical simulations. OS analyzed the numerical results and prepared the manuscript.

Competing interests. The authors declare that they have no conflict of interest.

References

Abramowitz, M. and Stegun, I. A.: Handbook of Mathematical Functions with Formulas, Graphs, and Mathematical Tables, vol. 56 of *National Bureau of Standards Applied Mathematics Series*, Dover, https://doi.org/10.1119/1.15378, 1964.

Bosler, P., Wang, L., Jablonowski, C., and Krasny, R.: A Lagrangian particle/panel method for the barotropic vorticity equations on a rotating sphere, Fluid Dynamics Research, 46, 031 406, 2014.

Chelton, D. B., Deszoeke, R. A., Schlax, M. G., El Naggar, K., and Siwertz, N.: Geographical variability of the first baroclinic Rossby radius of deformation, Journal of Physical Oceanography, 28, 433–460, 1998.

De-Leon, Y. and Paldor, N.: Zonally propagating wave solutions of Laplace Tidal Equations in a baroclinic ocean of an aqua-planet, Tellus A, 63, 348–353, https://doi.org/10.1111/j.1600-0870.2010.00490.x, 2011.

Garfinkel, C. I., Fouxon, I., Shamir, O., and Paldor, N.: Classification of eastward propagating waves on the spherical Earth, Quarterly Journal of the Royal Meteorological Society, 143, 1554–1564, 2017.

Gildor, H., Paldor, N., and Ben-Shushan, S.: Numerical simulation of harmonic, and trapped, Rossby waves in a channel on the midlatitude β-plane, Quarterly Journal of the Royal Meteorological Society, 142, 2292–2299, 2016.

Golub, G. H. and Welsch, J. H.: Calculation of Gauss quadrature rules, Mathematics of computation, 23, 221–230, 1969.

Haurwitz, B.: The motions of the atmospheric disturbances on the spherical earth, J. mar. Res, pp. 254–267, 1940.

Jablonowski, C.: Adaptive grids in weather and climate modeling, Ph.D. thesis, University of Michigan, Ann Arbor, MI, USA, 2004.

Jablonowski, C. and Williamson, D. L.: A baroclinic instability test case for atmospheric model dynamical cores, Quarterly Journal of the Royal Meteorological Society, 132, 2943–2975, 2006.

Jablonowski, C., Oehmke, R. C., and Stout, Q. F.: Block-structured adaptive meshes and reduced grids for atmospheric general circulation models, Philosophical Transactions of the Royal Society of London A: Mathematical, Physical and Engineering Sciences, 367, 4497–4522, 2009.

Lauritzen, P. H., Jablonowski, C., Taylor, M. A., and Nair, R. D.: Rotated versions of the Jablonowski steady-state and baroclinic wave test cases: A dynamical core intercomparison, Journal of Advances in Modeling Earth Systems, 2, 2010.

Li, X., Peng, X., and Li, X.: An improved dynamic core for a non-hydrostatic model system on the Yin-Yang grid, Advances in Atmospheric Sciences, 32, 648–658, 2015.

Matsuno, T.: Quasi-geostrophic motions in the equatorial area, Journal of the Meteorological Society of Japan. Ser. II, 44, 25–43, 1966.

Mohammadian, A. and Marshall, J.: A "vortex in cell" model for quasi-geostrophic, shallow water dynamics on the sphere, Ocean Modelling, 32, 132–142, 2010.

Paldor, N., De-Leon, Y., and Shamir, O.: Planetary (Rossby) waves and inertia–gravity (Poincaré) waves in a barotropic ocean over a sphere, Journal of Fluid Mechanics, 726, 123–136, 2013.

Phillips, N. A.: Numerical integration of the primitive equations on the hemisphere, Monthly Weather Review, 87, 333–345, https://doi.org/10.1175/1520-0493(1959)087<0333:NIOTPE>2.0.CO;2, 1959.

Polvani, L. M., Scott, R., and Thomas, S.: Numerically converged solutions of the global primitive equations for testing the dynamical core of atmospheric GCMs, Monthly weather review, 132, 2539–2552, 2004.

Press, W. H., Teukolsky, S. A., Vetterling, W. T., and Flannery, B. P.: Numerical recipes 3rd edition: The art of scientific computing, Cambridge university press, 2007.

Shamir, O. and Paldor, N.: A quantitative test case for global-scale dynamical cores based on analytic wave solutions of the shallow-water equations, Quarterly Journal of the Royal Meteorological Society, 142, 2705–2714, 2016.

Ullrich, P. A.: A global finite-element shallow-water model supporting continuous and discontinuous elements, Geoscientific Model Development, 7, 3017–3035, 2014.

Ullrich, P. A., Melvin, T., Jablonowski, C., and Staniforth, A.: A proposed baroclinic wave test case for deep-and shallow-atmosphere dynamical cores, Quarterly Journal of the Royal Meteorological Society, 140, 1590–1602, 2014.

Wheeler, M. and Kiladis, G. N.: Convectively coupled equatorial waves: Analysis of clouds and temperature in the wavenumber–frequency domain, Journal of the Atmospheric Sciences, 56, 374–399, 1999.

Williamson, D. L., Drake, J. B., Hack, J. J., Jakob, R., and Swarztrauber, P. N.: A standard test set for numerical approximations to the shallow water equations in spherical geometry, Journal of Computational Physics, 102, 211–224, https://doi.org/10.1016/S0021-9991(05)80016-6, 1992.